Multivariable Robust Control of the Plasma Rotational Transform Profile for Advanced Tokamak Scenarios in DIII-D

Wenyu Shi, William Wehner, Justin Barton, Mark D. Boyer, Eugenio Schuster, Didier Moreau, Tim C. Luce, John R. Ferron, Michael L. Walker, David A. Humphreys, Ben G. Penaflor and Robert D. Johnson

Abstract— **The tokamak is a high order, distributed parameter, nonlinear system with a large number of instabilities. Therefore, accurate theoretical plasma models are difficult to develop. However, linear plasma response models around a particular equilibrium can be developed by using data-driven modeling techniques. This paper introduces a linear model of the rotational transform ι profile evolution based on experimental data from the DIII-D tokamak. The model represents the response of the ι profile to the electric field due to induction as well as to heating and current drive (H&CD) systems. The control goal is to use both induction and H&CD systems to regulate the plasma ι profile around a particular target profile. A singular value decomposition (SVD) of the plasma model at steady state is carried out to decouple the system and identify the most relevant control channels. A mixed sensitivity H_∞ control design problem is formulated to synthesize a stabilizing feedback controller without input constraint that minimizes the reference tracking error and rejects external disturbances with minimal control energy. The feedback controller is then augmented with an anti-windup compensator, which keeps the given profile controller well-behaved in the presence of magnitude constraints in the actuators and leaves the nominal closed-loop unmodified when no saturation is present. Finally, computer simulations and experimental results illustrate the performance of the model-based profile controller.**

I. Introduction

The planned ITER tokamak [1] will be capable of exploring advanced tokamak (AT) modes of operation, which allow for steady-state operation. The tight requirements of AT modes motivates researchers to improve the modeling of the plasma response as well as the design of feedback controllers. The shape of the plasma current profile, which is intimately related to the rotational transform ι profile, is critical for the the creation of self-generated non-inductive current, which in turn serves as the enabler for steady-state operation. Recent experiments in different tokamaks (JET [2], JT-60U [3], DIII-D [4]) have demonstrated significant progress towards current profile control.

As an alternative to first-principles modeling, data-driven modeling methods [5] have been successfully used to develop linear dynamic models around a particular plasma equilibrium. In the JET tokamak, a two-time-scale linear system has been used to describe the magnetic and kinetic profiles around certain quasi-steady-state trajectories [2]. In discharges at the JT-60U tokamak, the momentum transport equation of the toroidal rotation profile has been estimated from transient data obtained by modulating the momentum source [3], [6]. System identification experiments have also been carried out on the DIII-D tokamak [6], and a data-driven model for the toroidal rotation profile [7] has been proposed.

In this paper, a data-driven linear dynamic model for the plasma rotational transform ι profile is identified from DIII-D data [6], and a robust, model-based, multi-input-multi-output (MIMO) controller for ι profile regulation during the current flat-top phase in a H-mode discharge is proposed. A singular value decomposition (SVD) [8], [9] is used to decouple the system and identify the most relevant control channels. The mixed sensitivity H_∞ control method [10] is applied to synthesize a closed-loop controller that minimizes the reference tracking error and rejects external disturbances with minimal control energy. The feedback controller is then augmented with an anti-windup compensator [11], [12], which keeps the given ι profile controller well-behaved in the presence of actuator constraints and leaves the nominal closed-loop unmodified when no saturation in the actuators is present. The proposed controller is successfully tested in computer simulations and experiments in DIII-D.

This paper is organized as follows. In Section II, the system identification process of the DIII-D tokamak is briefly described, and a linear model relating the safety factor ι profile to the plasma current (I_p), neutral beam injection (NBI), and electron cyclotron current drive (ECCD) is developed. In Section III, the design of the plasma control algorithm and the anti-windup compensator is described. Computer simulation and experimental results from DIII-D are presented in Section IV. Section V states the conclusions.

II. System Identification on DIII-D

System identification for the plasma rotational transform profile $\iota(\hat{\rho})$ was carried out with 5 Galerkin coefficients computed at normalized radius coordinate $\hat{\rho} = 0.2, 0.4, 0.5, 0.6, 0.8$, starting at $t = 2.6s$. The $\iota(\hat{\rho})$ profile is defined as the inverse of the safety factor $q(\hat{\rho})$ profile, where q is the ratio of the number of times a magnetic field line goes toroidally (the long way) around the tokamak to the number of times it goes around poloidally (the short way). The parameter $\hat{\rho}$ is the normalized minor radius, which can be denoted as $\hat{\rho} = \frac{\rho}{\rho_b}$, where ρ is the mean geometric minor

This work was supported in part by the National Science Foundation CAREER Award program (ECCS-0645086), the U.S. Department of Energy (DE-FG02-09ER55064, DE-FC02-04ER54698) and the European Communities under the contract of association between EURATOM and CEA (European Fusion Development Agreement). W. Shi (wenyu.shi@lehigh.edu), W. Wehner, J. Barton, M.D. Boyer and E. Schuster are with the Department of Mechanical Engineering and Mechanics, Lehigh University, Bethlehem, PA 18015, USA. D. Moreau is with CEA, IRFM, 13108 Saint-Paul-lez-Durance, France. T.C. Luce, J.R. Ferron, M.L. Walker, D.A. Humphreys, B.G. Penaflor, and R.D. Johnson are with General Atomics, San Diego, CA 92121, USA.

radius of the flux surface, i.e., $\pi B_{\phi,0}\rho^2 = \Phi$. The parameter Φ is the enclosed toroidal magnetic flux, and $B_{\phi,0}$ is the magnetic field at the geometric major radius. The parameter ρ_b is the minor radius of the last closed magnetic flux surface.

To collect the data for system identification a number of discharges were run with identical ramp-up phases and during the flat-top phase various actuators were modulated around the reference values [6]. The neutral beam injection (NBI) and electron cyclotron (EC) heating and current drive (H&CD) systems were used in these experiments. Available beam-lines (NBI) and gyrotrons (EC) were grouped to form, together with I_p, five independent H&CD actuators: (*i*) plasma current I_p, (*ii*) co-current NBI power P_{CO}, (*iii*) counter-current NBI power P_{CT}, (*iv*) balanced NBI power P_{BL}, and (*v*) total ECCD power from all gyrotrons P_{ECCD}. All actuators were modulated individually in open loop while the other actuators were held at their respective reference values.

The relation between inputs and outputs for any shot can be assumed in the form of

$$\iota(t) = \bar{\iota} + \Delta\iota(t) = \bar{G}(\bar{u}) + P\Delta u(t), \tag{1}$$

where $\bar{G}$ represents the relationship between the reference feedforward input $\bar{u}$ and reference feedforward output $\bar{\iota}$, $\Delta\iota$ is the feedback output defined as $\Delta\iota = \iota - \bar{\iota}$, and Δu is the feedback input which is defined as $\Delta u = u - \bar{u} = [\Delta I_p\ \Delta P_{CO}\ \Delta P_{CT}\ \Delta P_{BL}\ \Delta P_{ECCD}]^T$ for $u \in \{I_p, P_{CO}, P_{CT}, P_{BL}, P_{ECCD}\}$. By subtracting the feedforward value from our data set, we only consider the linear dynamics $\Delta\iota(t) = P\Delta u(t)$. The linear model P according to a least squares fit criterion is identified from experimental data using the prediction error method (PEM) [5]. The identified feedback model P can be expressed in the state space form

$$\dot{x} = Ax(t) + B\Delta u(t), \qquad \Delta y(t) = Cx(t) \tag{2}$$

where the state vector $x(t)$ and output vector $\Delta y(t)$ are defined as $x(t) = \Delta y(t) = \Delta\iota = \iota(t) - \bar{\iota}$, and the C matrix is the identity matrix. More details on the system identification procedure can be obtained from our previous work [6], [7].

III. Control System Design

A. Control System Structure

A MIMO robust controller based on the linear data-driven model (2) is described in this section. The ι profile control design procedure is summarized by the following steps: (1) decouple the system and identify the most relevant control channels, described in Section III-B, (2) design a H_∞ controller K ignoring control input saturation, described in Section III-C, (3) add the anti-windup compensator AW to minimize the adverse effect of any control input saturation on closed loop performance, described in Section III-D.

B. Singular Value Decomposition

The purpose of the feedback controller is to force the control output $\Delta y = y - \bar{y}$ to follow the target $\Delta y_{tar} = y_{tar} - \bar{y}$, therefore the tracking error is defined as $e(t) = \Delta y_{tar}(t) - \Delta y(t) - \Delta y_d$. The parameter y is the ι value at the normalized radius coordinate, i.e., $y(t) = [\iota(0.2,t)\ \iota(0.4,t)\ \iota(0.5,t)\ \iota(0.6,t)\ \iota(0.8,t)]^T$, $y_{tar}(t)$ is the desired target trajectory, $\bar{y}$ is the reference values obtained from the reference shot, and Δy_d is the output disturbance. The control goal is to guarantee closed-loop stability and improve performance while minimizing a quadratic cost function that weights the tracking error.

The relation between the inputs and the outputs in the linear model (2) can be expressed in terms of its transfer function $P(s)$, i.e.,

$$\frac{\Delta Y(s)}{\Delta U(s)} = P(s) = C(sI - A)^{-1}B \tag{3}$$

where s denotes the Laplace variable and $\Delta Y(s)$ and $\Delta U(s)$ denote the Laplace transforms of the output and the input vectors respectively. Assuming a constant target $\Delta\bar{y}_{tar}$ and closed-loop stabilization, the system can be maintained at steady state around the equilibrium. Therefore, the closed-loop system is specified by

$$\Delta\bar{y} = \bar{P}\Delta\bar{u} = -CA^{-1}B\Delta\bar{u} \quad \Delta\bar{u} = \bar{\hat{K}}\bar{e} = \bar{\hat{K}}\left(\Delta\bar{y}_{tar} - \Delta\bar{y}\right), \tag{4}$$

where $\Delta\bar{y}$ is the steady state output, $\Delta\bar{u}$ is the steady state input, $\bar{P}$ is the steady state transfer function (i.e. $s \to 0$), and $\hat{K}(s)$ represents the transfer function of the to-be-designed controller and $\bar{\hat{K}} = \hat{K}(0)$.

We consider the problem of minimizing a steady-state cost function given by

$$\bar{J} = \lim_{t\to\infty} e^T(t)Qe(t) = \bar{e}^T Q\bar{e} \tag{5}$$

where $\bar{e} = \Delta\bar{y}_{tar} - \Delta\bar{y}$, and $Q \in \Re^{p\times p}$ is a symmetric positive definite weighting matrix and p is the number of outputs. In order to weight the control effort, another positive definite weighting matrix $R \in \Re^{m\times m}$ is also introduced where m is the number of inputs. We then define the "weighted" steady-state transfer function, and its singular value decomposition (SVD), as $\tilde{P} = Q^{1/2}\bar{P}R^{-1/2} = USV^T$, where $S = \mathrm{diag}(\sigma_1, \sigma_2, \cdots, \sigma_m) \in \Re^{m\times m}$, $U \in \Re^{p\times m}$ ($U^TU = I$), and $V \in \Re^{m\times m}$ ($V^TV = VV^T = I$). The steady-state input-output relation is now expressed as

$$\Delta\bar{y} = Q^{-1/2}\tilde{P}R^{1/2}\Delta\bar{u} = Q^{-1/2}USV^TR^{1/2}\Delta\bar{u}. \tag{6}$$

By invoking the properties of the SVD, we note that the columns of the matrix $Q^{-1/2}US$ define a basis for the subspace of obtainable steady-state output values. Therefore, we can always write

$$\Delta\bar{y} = Q^{-1/2}US\Delta\bar{y}^* \iff \Delta\bar{y}^* = S^{-1}U^TQ^{1/2}\Delta\bar{y} \tag{7}$$

where $\Delta\bar{y}^* \in \Re^m$. This implies that we will only be able to track the component of the reference vector $\Delta\bar{y}_{tar}$ that lies in this subspace. We now write the reference vector as the sum of trackable components $\Delta\bar{y}_{tar_t}$ and non-trackable components $\Delta\bar{y}_{tar_{nt}}$, i.e., $\Delta\bar{y}_{tar} = \Delta\bar{y}_{tar_t} + \Delta\bar{y}_{tar_{nt}}$, where

$$\Delta\bar{y}_{tar_t} = Q^{-1/2}US\Delta\bar{y}^*_{tar} \iff \Delta\bar{y}^*_{tar} = S^{-1}U^TQ^{1/2}\Delta\bar{y}_{tar} \tag{8}$$

with $\Delta\bar{y}^*_{tar} \in \Re^m$ and $S^{-1}U^TQ^{1/2}\Delta\bar{y}_{tar_{nt}} = 0$. By defining $\Delta\bar{u}^* = V^TR^{1/2}\Delta\bar{u}$, the relationship between $\Delta\bar{y}^*$ and $\Delta\bar{u}^*$ is obtained by using (6) as

$$\Delta\bar{y}^* = S^{-1}U^TQ^{1/2}\Delta\bar{y} = S^{-1}U^TQ^{1/2}Q^{-1/2}USV^TR^{1/2}\Delta\bar{u} = \Delta\bar{u}^*$$

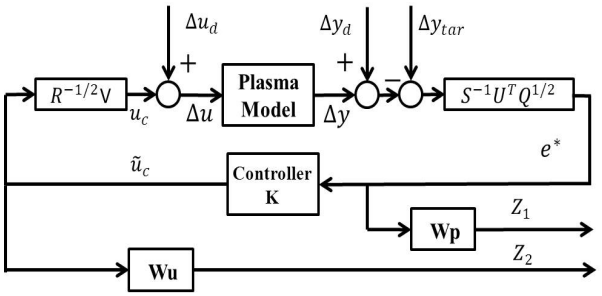

Fig. 1. H_∞ control formulation.

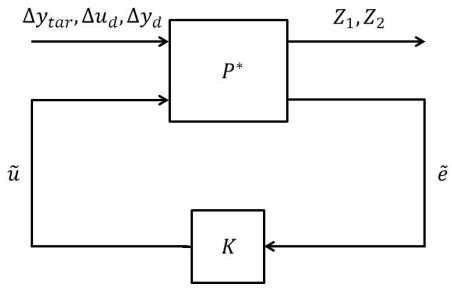

Fig. 2. Model in $P^* - K$ control framework.

and a one-to-one relationship between the inputs and outputs is obtained. The new system is a square decoupled system. The steady state error is now written as

$$\bar{e} = \Delta\bar{y}_{tar} - \Delta\bar{y} = Q^{-1/2}US(\Delta\bar{y}^*_{tar} - \Delta\bar{y}^*). \tag{9}$$

Substituting this expression into (5), the performance index is expressed as

$$\bar{J} = (\Delta\bar{y}^*_{tar} - \Delta\bar{y}^*)^T S^2 (\Delta\bar{y}^*_{tar} - \Delta\bar{y}^*) = \sum_{i=1}^{m} \sigma_i^2 (\Delta\bar{y}^*_{tar_i} - \Delta\bar{y}^*_i)^2.$$

The goal of the profile controller is to minimize the performance index $\bar{J}$.

C. Design of the Mixed Sensitivity H_∞ Controller

The mixed sensitivity H_∞ method is used to design the plasma ι profile controller. The design is based on the decoupled plasma model described above and ignores control input saturation. The structure of the proposed controller is shown in Fig. 1, where two frequency-dependent weighting functions W_p and W_u are introduced. The signals of the general control configuration are defined as the control input $\tilde{u} = \tilde{u}_c$, the tracking error $\tilde{e} = e^* = \Delta y^*_{tar} - \Delta y^* - \Delta y^*_d$, the exogenous reference $\tilde{r} = \Delta y_{tar}$, and the external performance signal $\tilde{z} = [Z_1,\ Z_2]^T$.

The feedback system shown in Fig. 1, now expressed in the conventional $P^* - K$ robust control framework, is shown in Fig. 2, where P^* is the generalized plant and K is the feedback controller. Using the Laplace Transform we can obtain a frequency-domain representation of the overall system. The plant $P^*(s)$ is the transfer function from the input signals $[\Delta y^T_{tar},\ \Delta u^T_d,\ \Delta y^T_d,\ \tilde{u}^T,]^T$ to the output signals $[Z_1^T,\ Z_2^T,\ \tilde{e}^T]^T$ and expressed as

$$\begin{bmatrix} Z_1 \\ Z_2 \\ \hline \tilde{e} \end{bmatrix} = P^*(s) \begin{bmatrix} \Delta y_{tar} \\ \Delta u_d \\ \Delta y_d \\ \hline \tilde{u} \end{bmatrix} = \left[\begin{array}{c|c} \tilde{P}_{11}(s) & \tilde{P}_{12}(s) \\ \hline \tilde{P}_{21}(s) & \tilde{P}_{22}(s) \end{array}\right] \begin{bmatrix} \Delta y_{tar} \\ \Delta u_d \\ \Delta y_d \\ \hline \tilde{u} \end{bmatrix}$$

$$\tilde{u} = K(s)\tilde{e} \tag{10}$$

The closed-loop transfer function from $[\Delta y^T_{tar},\ \Delta u^T_d,\ \Delta y^T_d]^T$ to $\tilde{z}$ is given by the lower linear fractional transformation (LFT), i.e.,

$$T_{zw} = F_l(P^*, K) = \tilde{P}_{11} + \tilde{P}_{12}K(I - \tilde{P}_{22}K)^{-1}\tilde{P}_{21} \tag{11}$$

where

$$\begin{aligned}
\tilde{P}_{11} &= [P^*_{11},\ P^*_{12},\ P^*_{13}] \\
&= \begin{bmatrix} W_pS^{-1}U^TQ^{1/2} & -W_pS^{-1}U^TQ^{1/2}P & -W_pS^{-1}U^TQ^{1/2} \\ 0 & 0 & 0 \end{bmatrix} \\
\tilde{P}_{12} &= P^*_{14} = \begin{bmatrix} -W_pS^{-1}U^TQ^{1/2}PR^{-1/2}V \\ W_u \end{bmatrix} \\
\tilde{P}_{21} &= [P^*_{21},\ P^*_{22},\ P^*_{23}] \\
&= [S^{-1}U^TQ^{1/2} \ -S^{-1}U^TQ^{1/2}P \ -S^{-1}U^TQ^{1/2}] \\
\tilde{P}_{22} &= P^*_{24} = -S^{-1}U^TQ^{1/2}PR^{-1/2}V.
\end{aligned}$$

We define the transfer function M_s as

$$M_s = (I + S^{-1}U^TQ^{1/2}PR^{-1/2}VK)^{-1}S^{-1}U^TQ^{1/2}, \tag{12}$$

and write the closed-loop transfer function as

$$T_{zw} = F_l(P^*, K) = \begin{bmatrix} W_pM_s & -W_pM_sP & -W_pM_s \\ W_uKM_s & -W_uKM_s & -W_uKM_s \end{bmatrix}. \tag{13}$$

We seek a controller $K(s)$ that stabilizes the system and minimizes the H_∞ norm of the transfer function $T_{zw}(P^*, K)$ between $[\Delta y^T_{tar},\ \Delta u^T_d,\ \Delta y^T_d]^T$ and $\tilde{z}$, i.e.,

$$\min_{K(s)} \|T_{zw}(P^*, K)\|_\infty = \min_{K(s)} (\sup_{\omega} \bar{\sigma}[T_{zw}(P^*, K)(j\omega)])$$

where $\bar{\sigma}$ represents the maximum singular value. This statement defines a mixed sensitivity H_∞ control problem, where the goal is to minimize both the tracking error (W_pM_s), the control effort (W_uKM_s) and the input disturbance (W_pM_sP) at the same time. The weighting functions W_p and W_u are parameterized as

$$W_p(s) = (\frac{\frac{s}{M_1} + w_{b1}}{s + w_{b1}A_1})^2 K_p, \quad W_u(s) = (\frac{s + w_{b2}A_2}{\frac{s}{M_2} + w_{b2}})^2 K_u$$

where the coefficients M_i, A_i, w_{bi}, for $i = 1, 2$, as well as K_p and K_u, are design parameters in the H_∞ control synthesis.

Finally, the overall plasma rotational transform ι profile controller can be written as

$$\hat{K}(s) = \frac{U_c(s)}{E(s)} = R^{-1/2}VK(s)S^{-1}U^TQ^{1/2} \tag{14}$$

where $U_c(s)$ denotes the Laplace transform of $u_c(t)$, and $E(s)$ denotes the Laplace transform of $e(t)$. The contribution to the plant input by the ι profile controller is written as

$$\begin{aligned}
u_c &= [\Delta I_p \ \Delta P_{CO} \ \Delta P_{CT} \ \Delta P_{BL} \ \Delta P_{ECCD}]^T \\
&= \mathscr{L}^{-1}\{\hat{K}(s)E(s)\}
\end{aligned} \tag{15}$$

where $\mathscr{L}^{-1}$ denotes the inverse Laplace transform.

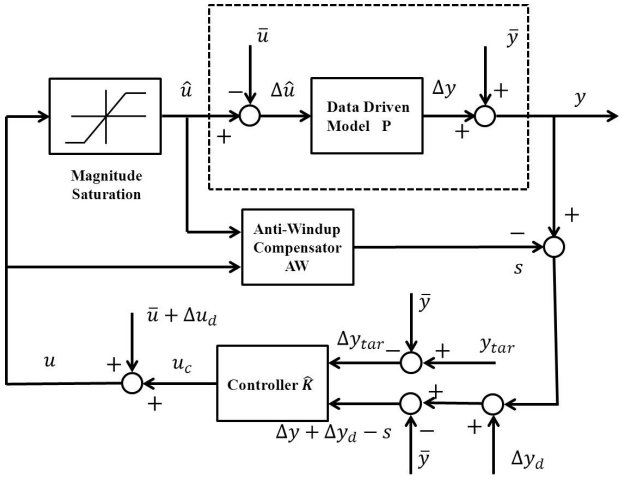

Fig. 3. DIII-D ι-profile control system architecture.

D. Design of the Anti-windup Compensator

The DIII-D tokamak is a nonlinear complex system, which is subject to actuator saturation. The input saturation of each channel is shown in Table I. At the moment of designing the H_∞ controller, the actuator saturations were not considered. As a result of saturation, the actual plant input may be different from the output of the controller. When this happens, the controller output does not drive the plant and as a result, the states of the controller are wrongly updated, which can cause the behavior of the system to deteriorate dramatically, or even become unstable.

The goal is not to redesign the MIMO controller but to design an anti-windup compensator that works with the H_∞ controller to keep it well-behaved and avoid undesirable oscillations when saturation is present. The anti-windup compensator must in addition leave the nominal closed-loop unmodified when no saturation is present.

The saturation function $\Delta\hat{u}$ is defined as

$$\Delta\hat{u} = sat_{\check{u}_{min}}^{\check{u}_{max}}(u_c) = \begin{cases} \check{u}_{max} & \text{if } \check{u}_{max} < u_c \\ u_c & \text{if } \check{u}_{min} < u_c < \check{u}_{max} \\ \check{u}_{min} & \text{if } u_c < \check{u}_{min} \end{cases} . \quad (16)$$

where $\check{u}_{max}$ and $\check{u}_{min}$ is the maximum and minimum saturation limit. From this, the dead-zone function can be defined as $Dz(u) = \Delta\hat{u} - u_c$. The plant P is the transfer function from the actual control input to the output, and plays an important part in anti-windup synthesis. The controller K is the original H_∞ controller, which has been designed such that its closed loop interconnection with P is stable.

When control signal saturation occurs, the anti-windup hides the saturation in magnitude from the nominal controller [11] and guarantees in this way that the controller remains well behaved. The anti-windup augmentation to the controller can be written as

$$\dot{x}_{aw} = A_{aw}x_{aw} + B_{aw}Dz(u)$$
$$s = C_{aw}x_{aw} + D_{aw}Dz(u)$$

When $\Delta\hat{u} = \Delta u$ we do not want the anti-windup to affect the system. To achieve this goal, we must have $s = 0$ and therefore $x_{aw} = 0$. However, due to the time scale of the model, the system will be affected by the anti-windup for an unnecessarily long time. The anti-windup augmentation can be written now as

$$\dot{x}_{aw} = A_{aw}x_{aw} + B_{aw}Dz(u) + \gamma(\Delta u, \Delta\hat{u})\lambda$$
$$s = C_{aw}x_{aw} + D_{aw}Dz(u) \quad (17)$$
$$\lambda = -cx_{aw} - A_{aw}x_{aw} - B_{aw}Dz(u)$$

where c is positive constant and $\gamma(\Delta u, \Delta\hat{u}) = 1$ if $\Delta u = \Delta\hat{u}$ and 0 otherwise. By choosing A_{aw}, B_{aw}, C_{aw}, and D_{aw} equal to the matrix of the plant P (3), we guarantee that x_{aw} will converge to zero fast and smoothly ($\dot{x}_{aw} = -cx_{aw}$) when $\Delta\hat{u} = \Delta u$, and so will s [11], [12].

The whole control system including the MIMO H_∞ controller and the anti-windup compensator is shown in Fig. 3. The proposed feedforward + feedback control scheme has been tested in simulations and experiments.

TABLE I

ACTUATOR LIMITS IN DIII-D

Channel	Actuator	Min	Max	Units
1	Ip	0.3	1.5	MA
2	Co-beam Power	0	12.5	MW
3	Ct-beam Power	0	2.5	MW
4	Blanced-beam Power	0	5.0	MW
5	Total ECCD Power	0.3	3.0	MW

TABLE II

THE H_∞ CONTROL PARAMETERS

Weight Function	M_i	w_{bi}	A_i	K_i
W_p	1	0.1	0.5	1
W_u	100	10	0.01	1

IV. SIMULATION AND EXPERIMENT RESULTS

In order to obtain relevant simulation results, we choose the same feedforward inputs and input disturbances in both experiment and simulation. In order to ensure that the target profile is close to the equilibrium used to obtain our model, a feedforward shot #146417 without feedback was run first with the same reference inputs as the shots used to identify the model. The reference inputs shown in Fig. 4 (dashed-dotted magenta lines) are $I_p = 0.9$ MA, $P_{CO} = 1.9838$ MW, $P_{CT} = 0$ MW, $P_{BL} = 2$ MW, and $P_{ECCD} = 1.4415$ MW. The target ι profile resulting from shot #146417 for these reference inputs are shown in Fig. 5 (dashed-dotted magenta lines). The input disturbances used to test the controller are $\delta I_p = 0.02$ MA, $\delta P_{CO} = -0.25$ MW, $\delta P_{CT} = 0$ MW, $\delta P_{BL} = -0.25$ MW, and $\delta P_{ECCD} = -0.1$ MW, and are applied at $t = 3.5$s. In the experiment, the counter-beam is not available, so it is off in the simulation too. The weight matrices Q and R are chosen to minimize the tracking error and optimize the control effort. Since the plasma current I_p plays the most significant role in the ι profile control, and the counter-current beam was not available in the experiment, the matrices are set as $Q = \text{diag}\begin{bmatrix} 1 & 1 & 1 & 1 & 1 \end{bmatrix}$ and $R = \text{diag}\begin{bmatrix} 0.1 & 0.25 & 1000 & 0.5 & 0.25 \end{bmatrix}$. The parameter c for the anti-windup compensator is set as 0.1. The co-beam value is distributed equally to the 15L and 33L beams, and the balanced-beam value is distributed to 15R and 21L beams in both experiment and simulation. In order to compare simulation and experimental results, we plot them in the same pictures (Fig. 4 and Fig. 5).

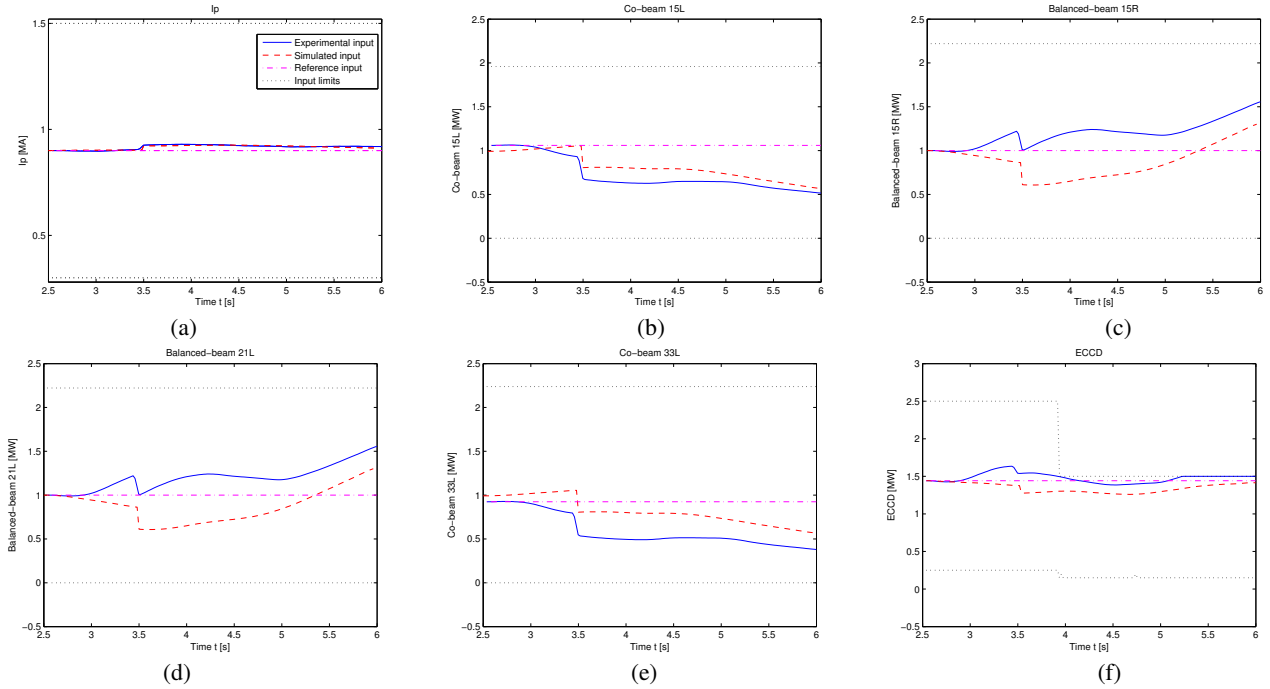

Fig. 4. Experimental and simulated control inputs.

A. Closed-loop Simulations

The closed-loop simulation is based on the linear data-driven model, which represents the ι profile evolution during the current flat-top phase in H-mode. In the closed-loop simulation, two goals should be achieved: (*i*) driving the system from an initial value to the target profile, and (*ii*) rejecting the input disturbance. In each case, the parameters for the H_∞ controller are shown in Table II. The experimental time interval associated with the plasma current flat-top phase is $[t_i,\ t_f] = [2.5,\ 6]$, and this same time interval is chosen for this simulation study.

In the first second of the simulation, the H_∞ controller effectively regulates ι around the target profile, afterwords the controller tries to reject the input disturbance. The simulated inputs (red dashed lines) are shown in Fig. 4. The controller rejects the disturbance in the plasma current I_p rather slowly, and the I_p nearly stays constant during the simulation, as shown in Fig. 4 (a). Beam values are shown in Fig. 4 (b), (c), (d) and (e), and they are not saturated. The limits of the total ECCD power were changed during the experiment, so the input of ECCD reaches the saturation and activates the anti-windup compensator in the last one second as shown in Fig. 4 (f). The simulated outputs (red dashed lines) are shown in Fig. 5. In the first second, the regulation results are very good for all control points. After the disturbance is switched on at 3.5 s, the controller reduces the tracking error to less than 10%.

B. Closed-loop Experiments on DIII-D

The controller described in Section III was active from $t = 2.5$ s, i.e., after 1 s of a 0.9 MA current flat-top. During the experiments, we concentrated on three main goals: (1) regulation of the plasma current during the current flat-top phase, (2) tracking control of the ι profile at 5 control points, and (3) input disturbance rejection.

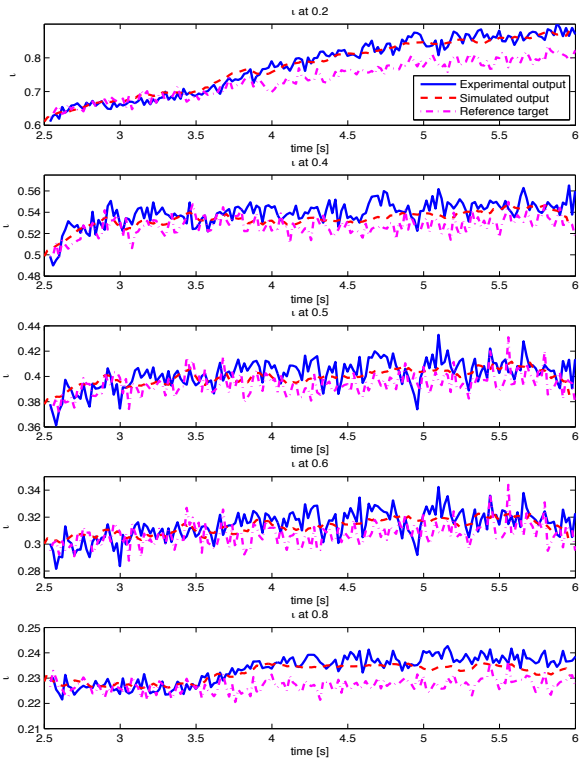

Fig. 5. Experimental and simulated ι at $\hat{\rho} = 0.2, 0.4, 0.5, 0.6, 0.8$.

The experimental inputs (solid blue lines) are shown in Fig. 4. The trend of all inputs is very similar to the simulation results, which means the data-driven linear model successfully approximates the DIII-D tokamak around the target profile. The experimental outputs (solid blue lines) are shown in Fig. 5. From $t = 2.5$ s to $t = 3.5$ s, there are no

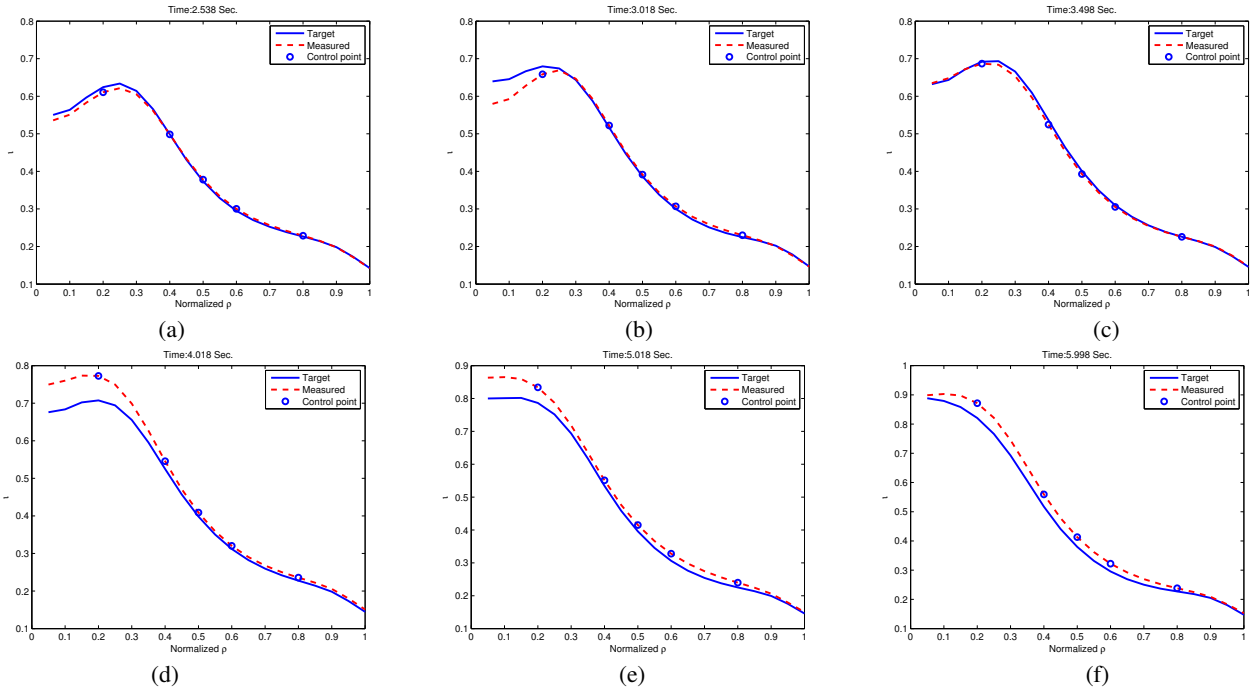

Fig. 6. Plasma $\iota(\hat{\rho})$ profile at time t= 2.538, 3.018, 3.498, 4.018, 5.018, 5.998 seconds from shot # 146419 on DIII-D.

input disturbances, and the tracking errors are less than 0.5%. The input disturbances were added at the experimental time $t = 3.5$s, and the influence is very clear from Fig. 4. The tracking quality clearly deteriorates after $t = 3.5$ s. However, the controller manages to drive the system within tolerable margins around the target profile. As in the simulation study, the plasma current I_p nearly keeps a constant value, which indicates the need to reduce its associated weight in R in future experiments for better tracking performance.

By requiring that the ι value be equal to the target value at the five control points defined by $\hat{\rho} = 0.2, 0.4, 0.5, 0.6, 0.8$, the controller forces the target ι profile to pass through the control points. In order to evaluate the ι profile at other points, a series of six plasma ι profiles at different times during the experiment are shown in Fig. 6. The blue line is the target profile, the red dash line is the measured profile, and the blue circles are the control points. As can be seen from Fig. 6 (a), (b), (c), the controller is able to keep the ι profile close to the target when there is no external input disturbance. After the input disturbances are applied to the system, the tracking errors become larger. As the time goes on, the controller attempts to reject the disturbance, and the errors become smaller, which is shown in Fig. 6 (d), (e), (f).

V. Conclusion

A robust, model-based, MIMO, ι-profile controller was designed for the DIII-D tokamak. The design was based on a linear, data-driven, plasma-response model around a reference profile during the current flat-top phase in H-mode. The feedback controller can regulate the system to the target, which is close to the reference equilibrium, even in the presence of various disturbances. Singular value decomposition of the steady state transfer function is used to decouple the system and identify the most relevant control channels. The mixed sensitivity H_∞ technique is used to minimize the tracking error and optimize input effort ignoring the saturation. Then an anti-windup compensator is applied to minimize the effects of any control input constraint. The proposed controller was tested experimentally in DIII-D, and preliminary results show potential for expanding present experimental control capabilities.

References

[1] A. Pironti and M. Walker, "Control of Tokamak Plasmas," *IEEE Control Systems Magazine*, vol. 25, no. 5, pp. 24–29, October 2005.

[2] D. Moreau, *et al.*, "A Two Time Scale Dynamic Model Approach for Magnetic and Kinetic Profile Control in Advanced Tokamak Scenarios on JET," *Nuclear Fusion*, vol. 48, pp. 1–38, 2008.

[3] Y. Yoshida, *et al.*, "Momentum Transport and Plasma Rotation Profile in Toroidal Direction in JT-60U L-mode Plasmas," *Nuclear Fusion*, vol. 47, no. 8, pp. 856–863, 2007.

[4] J. Ferron *et al.*, "Feedback Control of the Safety Factor Profile Evolution during Formation of an Advanced Tokamak Discharge," *Nucl. Fusion*, vol. 46, no. 10, pp. L13–17, 2006.

[5] L.Ljung, *System Identification: Theory for the User*. Prentice Hall PTR, 1999.

[6] D. Moreau, *et al.*, "Plasma Models for Real-time Control of Advanced Tokamak Scenarios," *Nuclear Fusion*, vol. 51, pp. 1–14, 2011.

[7] W. Wehner *et al.*, "Data-driven Modeling and Feedback Tracking Control of the Toroidal Rotation Profile for Advanced Tokamak Scenarios in DIII-D," in *Proceeding of the 2011 IEEE Multiconference on Systems and Control*, 2011.

[8] G. Ambrosino *et al.*, "Optimal Steady-state Control for Linear Non-right-invertible Systems," *IET Control Theory and Applications*, vol. 1, no. 3, pp. 604–610, 2007.

[9] ——, "Design and Implementation of an Output Regulation Controller for the JET Tokamak," *IEEE Transactions on Control Systems Technology*, vol. 16, no. 6, pp. 1101–1111, 2008.

[10] S. Skogested and I. Postlethwaite, *Multivariable Feedback Control*. John Wiley and Sons, Ltd, 2003.

[11] E. Schuster *et al.*, "Antiwindup Scheme for Plasma Shape Control with Rate and Magnitude Actuation Constraints in the DIII-D Tokamak," in *Proceeding of the 2003 IEEE International Conference on Decision and Control*, 2003.

[12] A. R. Teel, "Dynamic Anti-windup for Nonlinear Control Systems," *IEEE Transaction of Automatic Control*, 2004.